Influence of the laser cutting front geometry on the striation formation analysed with high-speed synchrotron X-ray imaging

To cite this article: Jannik Lind *et al* 2021 *IOP Conf. Ser.: Mater. Sci. Eng.* **1135** 012009

Influence of the laser cutting front geometry on the striation formation analysed with high-speed synchrotron X-ray imaging

Jannik Lind[1,2], Christian Hagenlocher[1], David Blazquez-Sanchez[2], Marc Hummel[3], A. Olowinsky[4], Rudolf Weber[1], Thomas Graf[1]

[1] Institut für Strahlwerkzeuge, University of Stuttgart, Pfaffenwaldring 43, 70569 Stuttgart, Germany

[2] Precitec GmbH & Co. KG, Draisstraße 1, 76571 Gaggenau, Germany

[3] Chair for Laser Technology LLT, RWTH Aachen University, Steinbachstraße 15,52074 Aachen, Deutschland

[4] Fraunhofer Institute for Laser Technology ILT, Steinbachstr. 15, 52074 Aachen, Germany

jannik.lind@ifsw.uni-stuttgart.de

Abstract. The generation of low surface roughness of the cut edge during laser beam cutting is a challenge. The striation pattern, which determines the surface roughness, can be distinguished into regular and interrupted striations, the latter resulting in an increased surface roughness. In order to analyse their formation, the space- and time-resolved cutting front geometry and melt film thickness were captured during laser beam fusion cutting of aluminium sheets with a framerate of 1000 Hz by means of high-speed synchrotron X-ray imaging. The comparison of the contours of the cutting fronts for a cut result with regular und interrupted striations shows that the contour fluctuates significantly more in case of interrupted striations. This leads to a strong fluctuation of the local angle of incidence. In addition, the average angle of incidence decreases, which results in an increase of the average absorbed irradiance. Both phenomena, local increase of absorbed irradiance and its dynamic fluctuation, result in a local increase of the melt film thickness at the cutting front which is responsible for the formation of the interrupted striations.

1. Introduction

The generation of low surface roughness of the cut edge during laser beam fusion cutting is challenging, especially when cutting thick metal sheets. In [1, 2] it was shown, that a low surface roughness coincides with a regular striation pattern, while a high surface roughness coincides with an interrupted striation pattern. An example of a cut edge in case of a regular striation pattern a) and for an interrupted striation pattern b) is shown in Figure 1. The origin of the coordinate system (x_c, y_c, z_c) was set at the intersection point of the beginning of the cut and the top surface of the cut edge. The relative

movement between the laser beam and the workpiece was performed by moving the workpiece against the x_c-direction, as highlighted by the black arrow. The difference of these patterns is that the striations do not run continuously from the top to the bottom surface of the sample in the case of interrupted striations, as indicated by the black dashed rectangle in Figure 1 b). Recent publications [3–6] identified local temperature maxima, which exceeded evaporation temperature, as a reason for the formation of the interrupted striation pattern. The local exceed of the evaporation temperature coincides with an increase of molten material, which flows not only in z_c-direction downward the cutting front, but also horizontally against the x_c-direction [7]. Furthermore, the thickness of the melt film and its flow exhibits strong instabilities [8–10]. Since the geometry of the cutting front influences the absorbed irradiance and therefore the temperature and melt film thickness, it is mandatory to know about the dynamic changes of the geometry of the cutting front and the melt film thickness during the transition from the process regime of regular striation to the regime of interrupted striation.

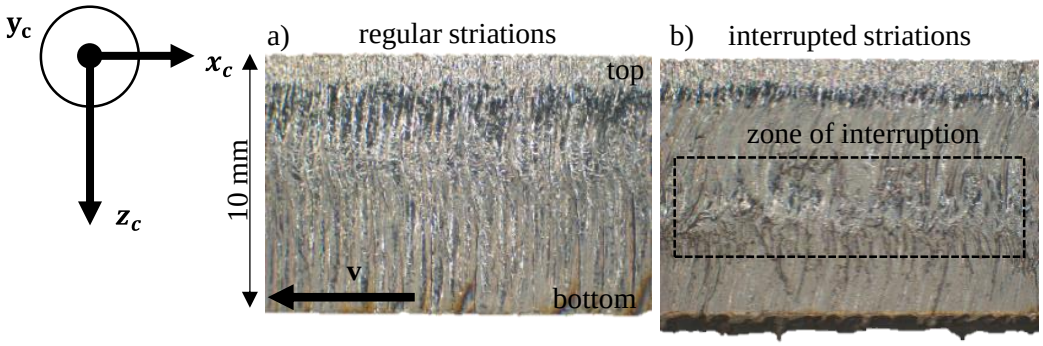

Figure 1 Regular striation pattern on the surface of the cut edge at a feed rate of v = 2.3 m/min a) and pattern with interrupted striations at an increased feed rate of v = 2.6 m/min b); P = 6 kW.

The space- and time-resolved in-process observation of the geometry of the cutting front was demonstrated in [11–13] by means of high-speed X-ray imaging. However, the presented approaches do not allow to observe the thickness of the melt film due to the used incoherent X-rays. By using coherent X-rays, it has been shown that the transition from the solid to the liquid physical state became visible during laser beam welding [14–20].

This paper presents for the first time a space- and time-resolved experimental determination of the geometry of the cutting front and melt film thickness during the transition from regular striation formation to interrupted striation formation within the same sample by means of high-speed synchrotron X-ray imaging.

2. Experimental Setup

Cutting of the aluminium alloy AlMg3 was investigated using a disk laser with a wavelength of 1.03 µm in combination with a *Precitec-ProCutterZoom2.0ET* cutting head. The beam-delivery fiber had a core diameter of 50 µm and the beam was focused to a waist diameter of approximately 150 µm to a top-hat intensity distribution with a Rayleigh-length of about 2.5 mm as measured with a Primes FocusMonitor. Figure 2 sketches the experimental setup, which was realized in cooperation with the RWTH in Aachen. The X-ray imaging system consisted of the DESY-synchrotron [21] providing the X-ray source (green), a scintillator (blue), and a high-speed camera (purple).

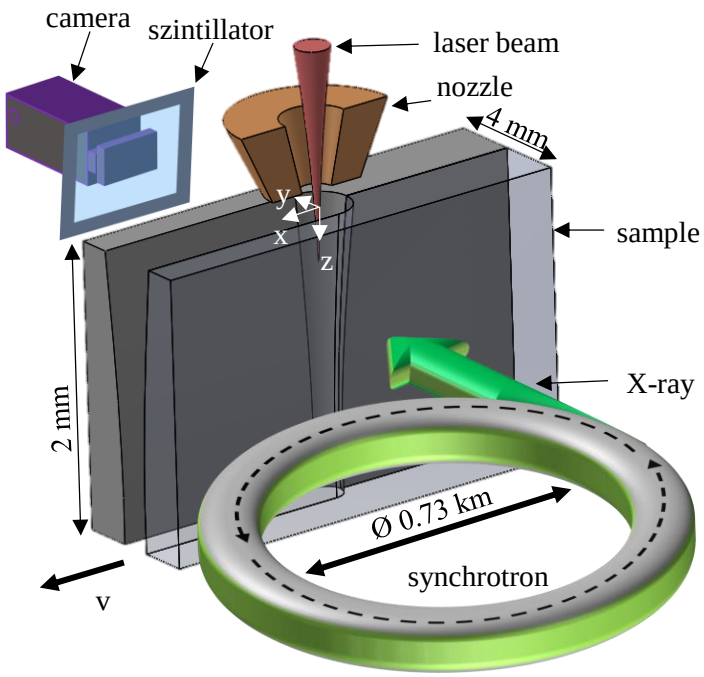

Figure 2 Sketch of the experimental setup.

The monochromatic X-ray beam from the electron accelerator ring DESY in Hamburg with an energy of 37.7 keV and an average beam diameter of approximately 3 mm transmitted the samples during the cutting process. Locally varying thickness due to the cutting kerf and locally varying attenuation coefficients depending on the physical state of the sample yielded a local attenuation of the beam. This locally attenuated X-ray projection behind the sample was converted by the scintillator to visible light which was recorded by the high-speed camera, in the following called "X-ray video". A similar system was previously used to study the laser cutting process using a microfocus tube as the X-ray source [11, 12]. However, the herein presented cutting process was observed by high-speed X-ray imaging in side-view at a frame rate of 1000 fps, with a spatial resolution of 256 pixels/mm and an image size of 920 x 920 pixels, resulting in an exposed area of approximately 3 mm in diameter. Due to the small divergence of the X-ray beam between 0.0055 mrad and 0.027 mrad, the impact of the penumbra to the observed blurring is negligible. The origin of the coordinate system (x, y, z) was set at the intersection point of the laser beam axis and the surface of the sample. The X-ray videos were post-processed with a flat-field correction. To be able to suitably observe the cutting process, aluminum was chosen as the sample material and the width of the samples (in the direction of the X-rays) was chosen to be 4 mm. Aluminum absorbs less X-rays than steel due to its lower attenuation coefficient, which allows for shorter exposure times of the X-ray images.

During the cutting process the nozzle (orange) with an outlet diameter of 3 mm was positioned 1 mm above the 2 mm thick samples. In order to observe the transition from regular to interrupted striation formation and to compare their formation differences, a critical process parameter regime was chosen for the synchrotron experiments at which regular and interrupted striations were generated within the same sample. This critical parameter were determined in previous work. The beam waist was positioned 2 mm above the sample's surface, the laser power was set to $P = 1$ kW, the feed rate was set to $v = 1.75$ m/min, and nitrogen with a pressure of 2 bar was used as the processing gas. The experiment within this critical process regime was repeated three times.

Figure 3 (Multimedia view [22]) shows an averaged image of 500 frames of an X-ray video recorded during one of the three repeated cutting processes. The frames were taken 500 ms after the beginning of the cutting process. The image shows the color-coded local transmittance of the X-ray radiation through the sample. A clear contrast between the solid sample material (blue, high absorption of X-rays) and the cutting kerf (red and orange, low absorption of X-rays) is visible in the images. Bright areas indicate a low local absorption of the X-rays and therefore a high local width of the cutting kerf. From these images, the geometry of the cutting front (line at the center of the cutting front) can be identified, as highlighted by the green dashed line in Figure 3. The position of the beam in the X-ray images was determined by applying a couple of laser pulses (0.8 ms at 1 kW and 588 Hz) on the sample. The symmetry axis of the resulting hole was defined as the position of the beam axis, which is represented by the white dash-dotted line in Figure 3. The caustic of the laser beam which results for the measured beam characteristics is represented by the white dashed line in Figure 3.

The transition from the solid to the liquid physical state causes interference effects of the transmitted coherent X-ray beam on the scintillator [23]. This interference effect results in a clearly visible transition from the solid to the liquid physical state, i.e. the liquidus isotherm, as marked by the black dashed line in Figure 3. Therefore, the width of the melt film in the x-direction can be derived.

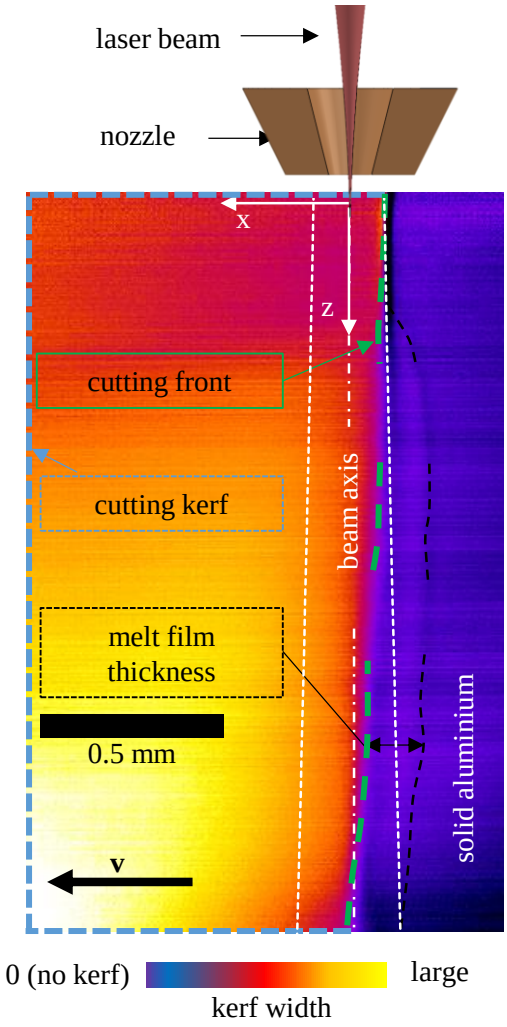

Figure 3 Average image of 500 frames from an X-ray video showing the cutting process in a 2 mm thick aluminium AlMg3 sheet. Red, yellow and white colored areas show the shape of the cutting front and cutting kerf. The black dashed line marks the liquidus isotherm; P = 1 kW, v = 1.75 m/min, Multimedia view [22].

3. Analysis of the transition from regular to irregular striations

3.1. Topography of the surface of the cut edge for regular and interrupted striations

In order to distinguish between regular and interrupted striations, Figure 4 presents the color-coded topography of the surface of the cut edge at the location of the transition from regular to interrupted striations within the same sample. The topography of the surface was measured with a scanner-based optical coherence tomography (OCT) system. Its setup and specifications are described in [24]. The dross at the bottom of the cut edge was not measured and is therefore not shown in Figure 4. The origin of the coordinate system (x_c, y_c, z_c) was set at the intersection point of the beginning of the cut and the top surface of the cut edge. The lower horizontal axis represents the time $t = x_c/v$ when the local position x_c of the presented cut edge was processed. Three lines parallel to the top surface of the cut edge were extracted for z_c = 0.25 mm (1), z_c = 1.00 mm (2), and z_c = 1.75 mm (3), as shown by the curves in Figure 4 bottom.

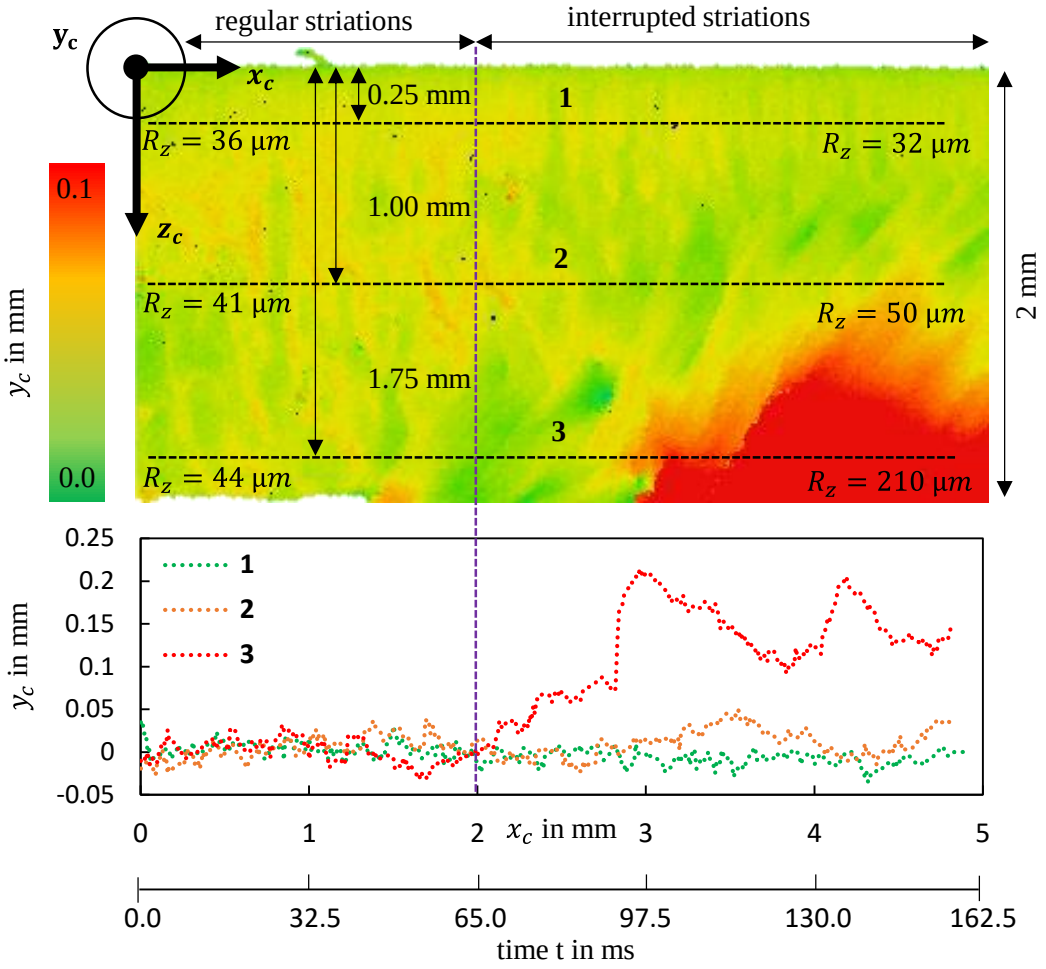

Figure 4 Topography image of the surface of the cut edge (top) and height profiles derived at three different z_c-positions (bottom). The vertical dashed purple line marks the transition from regular to interrupted striations within the same sample; P = 1 kW, v = 1.75 m/min.

The results show, that for x_c<2 mm, the height profile for all three measured positions is y_c<0.05 mm. For x_c>2 mm the height profile increases especially in the lower part (z_c = 1.75 mm) of the cut edge. The surface roughness R_z increases for x_c<2 mm from R_z=44 µm to R_z=210 µm for

x_c>2 mm. The vertical dashed purple line marks the transition from low to high surface roughness i.e. indication of the transition from regular to interrupted striations.

3.2. Geometry of the cutting front for regular and interrupted striations

During the cutting process the axis of the laser beam passed the position of the purple line in Figure 4 at the point in time t=65 ms, as indicated by the lower horizontal axis in Figure 4. Regular striations were generated on the surface of the cut edge for t<65 ms.

The contours of the cutting fronts during the formation of regular striations from 20 ms to 65 ms are represented with the curves in Figure 5a. The contours of the cutting fronts during the formation of interrupted striations at t>65 ms are represented with the curves in Figure 5b.

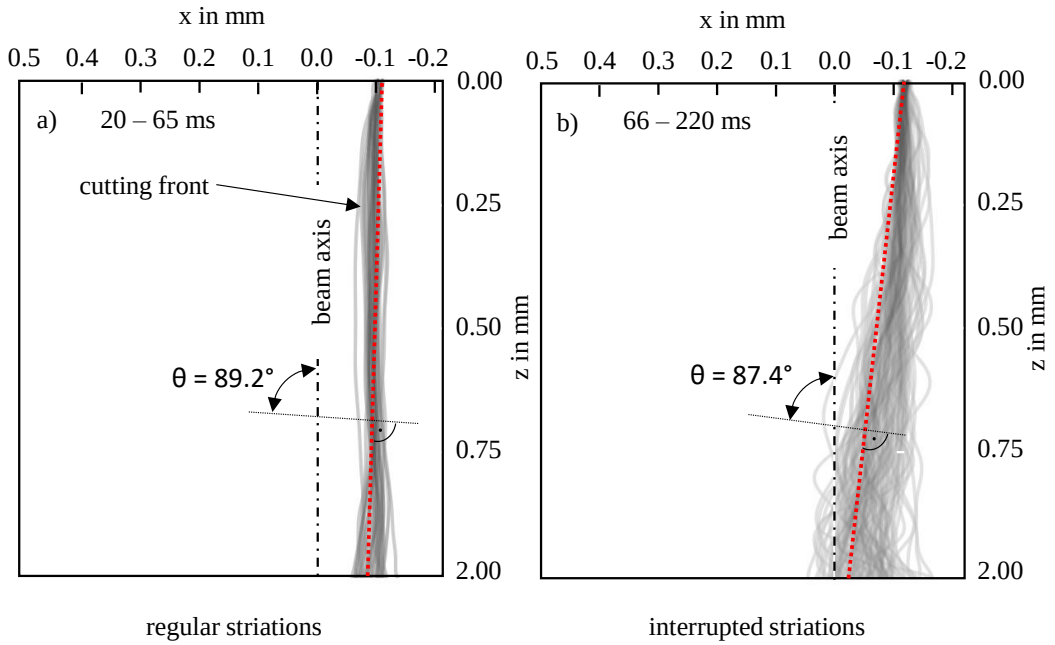

Figure 5 Contours of the center line of the cutting front along the cutting depth for cutting conditions with regular a) and interrupted b) striation formation; P = 1 kW, v = 1.75 m/min.

In the case of regular striations, the average angle of incidence θ on the cutting front with respect to the laser beam was 89.2°, as highlighted by the red dashed line in Figure 5. In the case of interrupted striations, the average angle of incidence θ decreases to 87.4° compared to the case of regular striations. When comparing the contours of the cutting fronts of the two cases, it can be seen that the fluctuation of the contour significantly increases in case of interrupted striations and therefore the local angle of incidence also changes more frequently. The absorbed irradiance of the laser beam increases with decreasing angle of incidence, as quantified in [11]. It is concluded that in case of interrupted striations, due to the smaller angles of incidence and the higher dynamic changes of the contour of the cutting front, the absorbed irradiance increases and changes more frequently.

3.3. Melt film thickness for regular and interrupted striations

In order to investigate the effect of the increase of the absorbed irradiance and of the fluctuations of the geometry of the cutting front, the melt film thickness at the cutting front was analyzed.

Figure 6 (Multimedia view [22]) shows six single images of an X-ray video of the cutting process in a 2 mm thick sheet of aluminium AlMg3 at different points in time (noted below). After 1359 ms the laser beam and the cutting gas were switched off. The good agreement of the liquidus isotherm (visible in the last frame at 1359 ms) and the recast layer in the longitudinal section verifies the capability to

determine the thickness of the melt film with high temporal and spatial resolution. For t<65 ms, regular striations were generated on the surface of the cut edge as indicated in Figure 4. During this period, the liquidus isotherm is not visible in the X-ray image. This indicates, that the melt film thickness is below the spatial resolution and thus smaller than approximately 30 µm in x-direction.

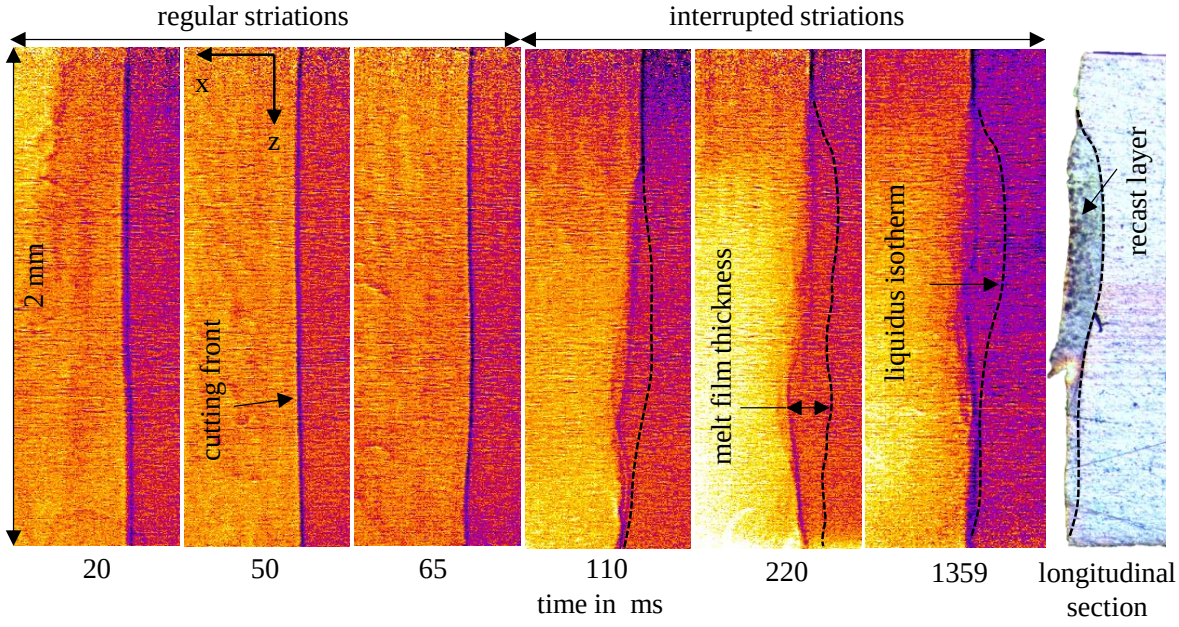

Figure 6 Single frames of an X-ray video of the cutting process in a 2 mm thick sheet of aluminium AlMg3 at six points in time (left) and longitudinal section of the cut front (right). Red, yellow and white colored areas show the shape of the cutting front and cutting kerf; P = 1 kW, v = 1.75 m/min, Multimedia view [22].

For t>65 ms, interrupted striations were generated on the surface of the cut edge and the liquidus isotherm can be identified as highlighted by the black dashed line. For z<0.25 mm, the melt film thickness is below the spatial resolution. For z>0.25 mm, the melt film thickness increases and temporal fluctuations occur. Since the frames contain motion blur at the position of the cutting front, it can be concluded that the geometry fluctuates with more than 1 kHz. It is concluded that in case of interrupted striations an increase of the melt film thickness coincides with the increase of the absorbed irradiance for t>65 ms.

4. Conclusion

This paper presents for the first time a space- and time-resolved experimental determination of the geometry of the cutting front and melt film thickness during the transition from regular striation formation to interrupted striation formation by means of high-speed synchrotron X-ray imaging.

The comparison of the contours of the cutting fronts for a cut result with regular und interrupted striations shows that the contour fluctuates significantly more in case of interrupted striations. This leads to a strong fluctuation of the local angle of incidence. In addition, the average angle of incidence decreases, which results in an increase of the average absorbed irradiance. Both phenomena, local increase of absorbed irradiance and its dynamic fluctuation, result in a local increase of the melt film thickness at the cutting front which is responsible for the formation of the interrupted striations.

Future work will focus on strategies to prevent the formation of interrupted striations based on the presented results.

5. Acknowledgement

This research was supported by Precitec GmbH & Co. KG and Trumpf GmbH & Co. KG. The presented investigations were carried out in cooperation with DESY in Hamburg and with RWTH Aachen University within the framework of the Collaborative Research Centre SFB1120-236616214 “Bauteilpräzision durch Beherrschung von Schmelze und Erstarrung in Produktionsprozessen” and funded by the Deutsche Forschungsgemeinschaft e.V. (DFG, German Research Foundation). We acknowledge DESY (Hamburg, Germany), a member of the Helmholtz Association HGF, for the provision of experimental facilities. Parts of this research were carried out at PETRA III and we would like to thank F. Beckmann and J. Moosmann for assistance in using P07 EH4. Beamtime was allocated for proposal I-20191140. The sponsorship and support is gratefully acknowledged.

6. ORCID iDs

J. Lind https://orcid.org/0000-0002-2196-5616
C. Hagenlocher https://orcid.org/0000-0003-2929-9723
D. Blazquez-Sanchez https://orcid.org/0000-0002-3504-229X
M. Hummel https://orcid.org/0000-0002-9097-9843
A. Olowinsky https://orcid.org/0000-0002-5231-8251
R. Weber https://orcid.org/0000-0001-8779-2343
T. Graf https://orcid.org/0000-0002-8466-073X

7. References

[1] Wandera C, Salminen A and Kujanpaa V 2009 *Journal of Laser Applications* **21** 154–61
[2] Bocksrocker O, Berger P, Fetzer F, Rominger V and Graf T 2019 *Lasers Manuf. Mater. Process.* **6** 1–13
[3] Bocksrocker O, Berger P, Kessler S, Hesse T, Rominger V and Graf T 2020 *Lasers Manuf. Mater. Process.* **7** 190–206
[4] Onuseit V, Ahmed M A, Weber R and Graf T 2011 *Physics Procedia* **12** 584–90
[5] Petring D 2016 *Proc of JLPS 84th Laser Materials Processing Conf Nagoya Japan*
[6] Onuseit V, Michael J, Weber R and Graf T 2011 *Proc. of Icaleo Paper 104*
[7] Olsen F 2006 *Laser materials processing conference ICALEO* 401
[8] Levichev N, Staudt T, Schmidt M and Duflou J R 2021 *CIRP Annals*
[9] Kaplan A FH 2015 *Optics and Lasers in Engineering* **68** 35–41
[10] Hirano K and Fabbro R 2011 *J. Phys. D: Appl. Phys.* **44** 105502
[11] Lind J, Fetzer F, Blazquez-Sanchez D, Weidensdörfer J, Weber R and Graf T 2020 *Journal of Laser Applications* **32** 32015
[12] Lind J, Fetzer F, Hagenlocher C, Blazquez-Sanchez D, Weber R and Graf T 2020 *Journal of Manufacturing Processes* **60** 470–80
[13] Ozaki H, Le M Q, Kawakami H, Suzuki J, Uemura Y, Doi Y, Mizutani M and Kawahito Y 2016 *Journal of Materials Processing Technology* **237** 181–7
[14] Simonds B J, Tanner J, Artusio-Glimpse A, Williams P A, Parab N, Zhao C and Sun T 2021 *Applied Materials Today* **23** 101049
[15] Wolff S J, Wu H, Parab N, Zhao C, Ehmann K F, Sun T and Cao J 2019 *Scientific reports* **9** 962
[16] Börner S, Dittrich D, Mohlau P, Leyens C, García-Moreno F, Kamm P H, Neu T R and Schlepütz C M 2021 *Journal of Laser Applications* **33** 12026
[17] Shevchik S, Le-Quang T, Meylan B, Farahani F V, Olbinado M P, Rack A, Masinelli G, Leinenbach C and Wasmer K 2020 *Scientific reports* **10** 3389
[18] Cunningham R, Zhao C, Parab N, Kantzos C, Pauza J, Fezzaa K, Sun T and Rollett A D 2019 *Science (New York, N.Y.)* **363** 849–52

[19] Miyagi M, Kawahito Y, Kawakami H and Shoubu T 2017 *Journal of Materials Processing Technology* **250** 9–15
[20] Wagner J, Hagenlocher C, Hummel M, Olowinsky A, Weber R and Graf T 2021 *Metals* **11** 797
[21] Schell N, King A, Beckmann F, Fischer T, Müller M and Schreyer A 2013 *MSF* **772** 57–61
[22] Lind J, Hagenlocher C, Blazquez-Sanchez D, Hummel M, Olowinsky A, Weber R and Graf T 2021 *High-speed synchrotron X-ray video of the laser beam cutting process in a 2 mm thick sheet of aluminium: https://doi.org/10.18419/darus-1824* 1st edn (DaRUS)
[23] van der Veen F and Pfeiffer F 2004 *J. Phys.: Condens. Matter* **16** 5003–30
[24] Holder D, Buser M, Boley S, Weber R and Graf T 2021 *Materials & Design* **203** 109567